Programmable Release | Hot Paper

International Edition: DOI: 10.1002/anie.201600383
German Edition: DOI: 10.1002/ange.201600383

Multicompartmental Microcapsules with Orthogonal Programmable Two-Way Sequencing of Hydrophobic and Hydrophilic Cargo Release

*Weinan Xu, Petr A. Ledin, Zacharoula Iatridi, Constantinos Tsitsilianis, and Vladimir V. Tsukruk**

Abstract: *Multicompartmental responsive microstructures with the capability for the pre-programmed sequential release of multiple target molecules of opposite solubility (hydrophobic and hydrophilic) in a controlled manner have been fabricated. Star block copolymers with dual-responsive blocks (temperature for poly(N-isopropylacrylamide) chains and pH for poly(acrylic acid) and poly(2-vinylpyridine) arms) and unimolecular micellar structures serve as nanocarriers for hydrophobic molecules in the microcapsule shell. The interior of the microcapsule can be loaded with water-soluble hydrophilic macromolecules. For these dual-loaded microcapsules, a programmable and sequential release of hydrophobic and hydrophilic molecules from the shell and core, respectively, can be triggered independently by temperature and pH variations. These stimuli affect the hydrophobicity and chain conformation of the star block copolymers to initiate out-of-shell release (elevated temperature), or change the overall star conformation and interlayer interactions to trigger increased permeability of the shell and out-of-core release (pH). Reversing stimulus order completely alters the release process.*

Microcapsules with high loading capacity and stimuli-responsive encapsulation-release behavior[1,2] are highly desirable for demanding applications in drug and gene delivery,[3] tissue engineering,[4] nanomedicine,[5] and as self-healing materials.[6] However, most reported microcapsules to date have simple or homogenous composition, which can load only one type of cargo molecule in their interior/shell under one stimulus. Concurrent or sequential loading and unloading which is important for biomolecular applications[7,8] cannot be realized in a traditional design.[9] Thus, next generation microcapsules with more complex loading-unloading behavior, so-called multicompartmental microcapsules, have been suggested.[10,11] The concept of multicompartmental microcapsules requires a different and hierarchical design for the shell and inner space of the microcapsule.

One common approach to fabricate multicompartmental microcapsules utilizes complex templates[12,13] such as porous microparticles and satellite nanoparticles.[14] For instance, porous calcium carbonate microparticles can be coated with a thin polymer shell, then polymer coated smaller particles can be assembled in the periphery of the large particles; multicompartmental microcapsules can be generated after dissolving all the template particles.[15] However, this method incurs irregular shapes, high polydispersity, and low yield. Another popular method to fabricate multicompartmental microcapsules is based on multi-flow microfluidic.[16] For instance, different components in the water and oil phases result in separate inclusion in the shell and core regions.[17,18] Complex structures fabricated in this way include multicore–shell and hole–shell morphologies.[19] Despite the advantages of the microfluidic technique in fabricating microcapsules, it is incapable of mass producing large numbers of microcapsules in a short time. Moreover, an adhesive oil layer is usually left on the surface of the prepared microcapsules, which potentially affects their properties and further surface modification.[20] Furthermore, the lower limit of the microcapsule size that can be fabricated cannot be very small due to the large size of the channels that compromises the long-term stability.[21] Finally, the incorporation of polymeric nanocarriers such as micelles and polymersomes in the shell is another way to fabricate multicompartmental microcapsules.[22,23] However, the stability of the nanocarriers can be compromised under a battery of different stimuli because the carriers are usually formed through weak non-covalent interactions.

Herein, we demonstrate novel microstructures with pre-programmed orthogonal release of different molecular loads, hydrophilic and hydrophobic molecules, from the interior and the shell of the microcapsules under different stimuli in direct and reversible sequences. Our method is based on the encapsulation ability of the polymeric building blocks in the shell,[24] namely, complex mutiblock responsive star polymers with a core–shell micellar structure.[25] The star polymers have a hydrophobic core and a dense thermal-responsive shell, allowing them to serve as nanocarriers for hydrophobic molecules within the shell.[26] A different kind of hydrophilic molecules can be encapsulated in the microcapsule interior by tuning the permeability of the shell (Figure 1 a).[27] By applying pH and temperature stimuli in different sequences, a sequential release of hydrophobic and hydrophilic model molecules can be achieved from different compartments. The ability to encapsulate multiple cargo molecules with very different orthogonal solubilities (such as hydrophilic and hydrophobic types) and release them on demand in a pre-programmed order from the responsive microcapsules is a unique feature of the microstructures suggested here.

The star-graft quarterpolymers (SGQP) utilized for this study are soft multi-block multi-responsive macromolecules (Figure 1 b).[28] The SGQP $PS_n[P2VP\text{-}b\text{-}(PAA\text{-}g\text{-}PNIPAM)]_n$ (PS: polystyrene, P2VP: poly(2-vinylpyridine), PAA: poly(acrylic acid)) contain two classes of arms, one is a shorter hydrophobic PS arm, the other is a pH responsive hydrophilic P2VP-*b*-PAA block copolymer arm with grafted PNIPAM chains on the PAA block (Figure 1 b; Supporting Information, Tables S1, S2). The center of the SGQP consists of a hydrophobic polydivinylbenzene (PDVB) core and short PS chains,[29] which means the SGQP have the potential to encapsulate hydrophobic molecules in the core. The grafting of poly(*N*-isopropylacrylamide) (PNIPAM) chains on the corona effectively shields the charges in the inner blocks, which can significantly extend their in vivo circulation for biomedical applications.[30]

The SGQP precursors were synthesized via a one-pot/four-step sequential "living" anionic polymerization procedure (an extended "in-out" method), which was described in detail elsewhere.[31] Briefly, *sec*-BuLi was used as the initiator to prepare "living" PS chains in the first step, then the PS chains were used to polymerize a small quantity of DVB,

[*] Dr. W. Xu, Dr. P. A. Ledin, Prof. V. V. Tsukruk
School of Materials Science and Engineering
Georgia Institute of Technology, Atlanta, GA (USA)
E-mail: vladimir@mse.gatech.edu
Dr. Z. Iatridi, Prof. C. Tsitsilianis
Department of Chemical Engineering
University of Patras, Patras (Greece)

Supporting information for this article can be found under: http://dx.doi.org/10.1002/anie.201600383.

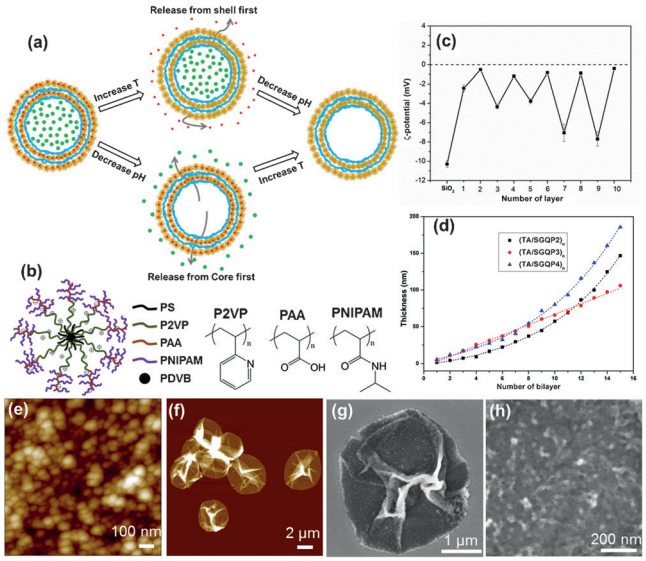

Figure 1. a) The programmable encapsulation and release of two types of molecules from the microcapsule core and shell regions. b) Chemical structure of the SGQP. c) ζ-potential as a function of the number of layers during LbL assembly on silica microparticles. d) Thickness increase with the number of bilayers for $(TA/SGQP)_n$ LbL films. e) Morphology of the $(TA/SGQP)_{15}$ LbL films, and f) $(TA/SGQP)_6$ microcapsules as measured by AFM; *Z* range is 100 nm for (e) and 800 nm for (f). g), h) SEM images of the microcapsules at different magnifications.

resulting in a living star-shaped PS bearing active sites in the PDVB core. Then the "living" star polymers were used to initiate polymerization of 2VP, leading to a second generation of P2VP arms. Finally, *tert*-butyl acrylate (*t*BA) was polymerized from the end of each P2VP arms. The PS_n(P2VP-*b*-PAA)$_n$ terpolymers were obtained after acidic hydrolysis of the P*t*BA blocks. To graft PNIPAM chains to the PAA blocks, PNIPAM-NH_2 chains were grafted to the carboxylate groups of PAA. Detailed information about the synthesis of the polymers can be found in a previous report.[32] The pH and temperature dual responsive properties of the SGQP in solution, including the interesting sol–gel phase behavior, were reported earlier.[32] The detailed molecular structure and their responsive behaviors at the air–water interface have also been studied earlier.[29]

Because the SGQP have a dense PNIPAM shell, which is able to form hydrogen bonding as acceptors, tannic acid (TA) was chosen as the hydrogen donor and a component for hydrogen bonded shell assembly (Supporting Information, Figure S2).[33] TA is a natural polyphenol, which has attracted much attention as a coating material in recent years due to its versatile chemistry.[34] TA is capable of forming a hydrogen bonding network for the fabrication of microcapsules.[35,36] The layer-by-layer (LbL) assembly is conducted on spherical substrates according to the usual procedure which results in hollow microcapsules after the core is dissolved.[37]

Electrophoresis experiments for monitoring the LbL assembly showed modest shifting of surface charge with the overall potential staying in the negative region, which is a characteristic of a hydrogen-bonded assembly process (Figure 1 c).[37] The surface potential varies between −2.4 mV to −7.7 mV when TA is the outmost layer, and is only slightly negatively charged (below −1.0 mV) when the SGQP constitutes the outermost layer. The thickness of the LbL films increases consistently with the number of layers in linear or exponential growth modes depending on the arm number and PNIPAM graft density (Figure 1 d,e; more discussion is given in the Supporting Information).[38] After core removal, the hollow microcapsules collapse in the dry state with formations of random wrinkles on the surface (Figure 1 f). As an example, AFM and SEM images of the $(TA/SGQP)_6$ microcapsules (6 stands for the number of bilayers) show a granular and porous surface morphology, also a common characteristic of hydrogen bonded LbL assemblies (Figure 1 g,h).[39] Cross-section analysis of the AFM images gives the thickness of these microcapsules (for instance, 36.1 ± 5.2 nm was measured for $(TA/SGQP)_6$ microcapsules) that matches very well the thickness of 6 bilayer planar film (37.2 nm).

The morphology and permeability of the (TA/SGQP) microcapsules are responsive to pH and temperature because of the corresponding properties of individual star macromolecules (Supporting Information, Figure S1).[32] To test the permeability of the shells, fluorescein isothiocyanate (FITC) labeled dextran with various molecular weights were used as fluorescent probes.[40] The permeability tests of the $(TA/SGQP)_6$ shells at different pH conditions to 150 kDa FITC-dextran are shown in Figure 2 and Table 1 (see also the Supporting Information, Figure S4). The microcapsules are fully and partially permeable at pH 3 and pH 5, respectively, and completely impermeable at pH 7. Considering that the hydrodynamic diameter of 150 kDa Dextran is around 20 nm,[41] we can conclude that the average mesh size of the

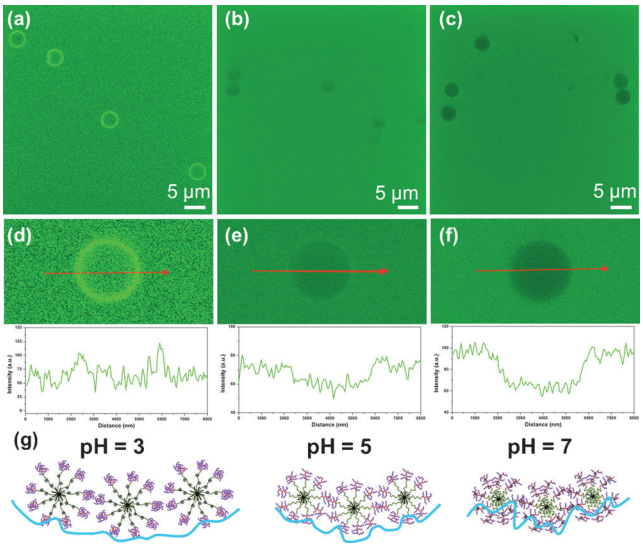

Figure 2. Permeability of $(TA/SGQP)_6$ microcapsules to 150 K FITC-dextran at a), d) pH 3, b), e) pH 5, c), f) pH 7. The plot below each image is the representative fluorescent intensity profile over the microcapsule. g) The structural changes of the microcapsule shell (only a portion of one bilayer is shown for clarity) at different pH conditions. Blue lines represent the TA layers.

Table 1: Permeability of $(TA/SGQP)_6$ microcapsules to FITC-Dextran with various molecular weights at different pH conditions.[a]

Sample	pH	FITC-Dextran 20 kDa	70 kDa	150 kDa	250 kDa	500 kDa
$(TA/SGQP)_6$	3	+	+	+	−	−
$(TA/SGQP)_6$	5	+	+	+/−	−	−
$(TA/SGQP)_6$	7	+	+	−	−	−

[a] + permeable, − not permeable, +/− partially permeable.

$(TA/SGQP)_6$ microcapsule shell is around 20 nm and highly dependent on pH.

The mechanism for the pH controlled permeability of the $(TA/SGQP)_6$ microcapsules is a combination of changes in the conformation of the SGQP and the hydrogen bonding interactions between TA and SGQP (Figure 2g).[29] At a low pH condition (pH 3), the P2VP blocks are highly charged and extended, the grafted PNIPAM chains interact with the PAA block via hydrogen bonding, so that the terminal block are collapsed. The fully extended inner block as well as the loose interaction between collapsed arm ends with TA gives the microcapsules high permeability. In contrast, when pH is increased to 7, the inner P2VP blocks are neutral and hydrophobic, and tend to collapse instead. The PAA blocks are highly negatively charged and expanded, resulting in the PNIPAM chains being well separated from the core. As a result, the SGQP have a condensed core region and an extended shell region, which results in significant decrease in permeability. At pH 5, both P2VP and PAA are partially charged, and thus the overall permeability is in between two extreme cases. The overall average size of the microcapsules also decreases from 3.93 μm at pH 3 to 3.59 μm at pH 7 (Supporting Information, Figure S5), due to the contraction of the SGQP and shell densification that affects the permeability.

As a next step, the ability of SGQP micelles as nanocarriers for hydrophobic molecules has been explored. We choose Nile Red (a hydrophobic fluorescent dye) as the model molecule for encapsulation into the core region of the SGQP, which is composed of hydrophobic PS and PDVB.[42] UV/Vis and fluorescence spectra of the SGQP after encapsulation of Nile Red show the strong characteristic peak of Nile Red (Supporting Information, Figure S6). Significant blue-shift indicates that Nile Red has been successfully encapsulated into hydrophobic environment.[43] Following this step, SGQP with encapsulated Nile Red have been used to prepare LbL microcapsules (Figure 1a). CLSM images of these $(TA/SGQP)_6$ microcapsules showed stable, well-defined red fluorescent shells, indicating the highly localized encapsulation of Nile Red dye (Figure 3a).

To initiate thermal-induced release, the microcapsule suspension was heated to 45 °C (higher than the LCST of PNIPAM) for 15 mins which resulted in complete release of the red dye from the shells without changing microcapsule morphology (Figure 3b,c). The temperature-induced release of Nile Red is primarily due to the change in hydrophobicity of the PNIPAM shell during LCST transition and increased thermal mobility of dye molecules.[44] As is known, above LCST, the PNIPAM blocks are transformed to a hydrophobic and collapsed state, which can stimulate the hydrophobic Nile Red to migrate to the PNIPAM shell region, and eventually diffuse out of the microcapsule shell. The release kinetics of Nile Red from the SGQP is also expected to be pH-dependent,[42] as discussed in the Supporting Information.

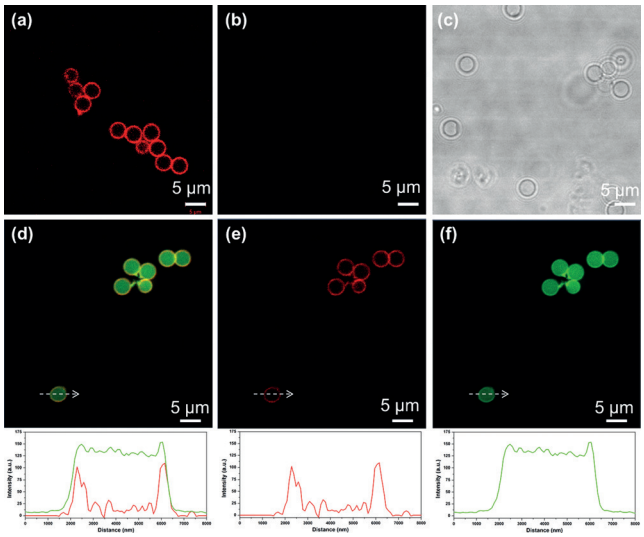

Figure 3. a) CLSM images of $(TA/SGQP)_6$ microcapsules with encapsulated Nile Red in the shell, b) CLSM images of the same sample after heating to 45 °C for 15 min, c) transmission mode image of the same area as (b). d) CLSM images of the $(TA/SGQP)_6$ microcapsules with encapsulated Nile Red in the shell and FITC-Dextran inside the microcapsules; e) red channel and f) green channel of the same area in the same sample. The plot below each image is the representative fluorescent intensity profile across the microcapsule.

Taking advantage of the pH and thermal dual responsive properties of SGQP, we conducted pre-encapsulation of Nile Red inside the SGQP within the shell followed by post-encapsulation of FITC-dextran inside the interior of the microcapsules (Supporting Information, Figure S7). The double-channel CLSM image shows successful dual-encapsulation: the microcapsule interior contains only green FITC-dextran and the red Nile Red only present on the shell of the microcapsules (Figure 3d). The separate red and green channel images show the multicompartmental and localized nature of the encapsulation process (Figure 3e,f).

Sequential release of the encapsulated target molecules can be achieved by tuning the internal structure and permeability of the $(TA/SGQP)_6$ shell (Figure 4). The entire programmable release process involves two independent steps and two possible paths (Figure 1a). First, the temperature increase triggers the efficient release of Nile Red from the SGQP in the shell, while the FITC-dextran remains encapsulated inside the microcapsules without any losses (Figure 4b). During the second stage, pH is decreased to 5 at room temperature which increases the permeability of the shell. This allows the FITC-dextran to be readily released from the microcapsule interior, leaving only some traces on the shell (Figure 4c; more discussion is given in the Supporting Information). The programmable release behavior is uniform for all the microcapsules in the system, as can be seen from larger area CLSM images with numerous microcapsules

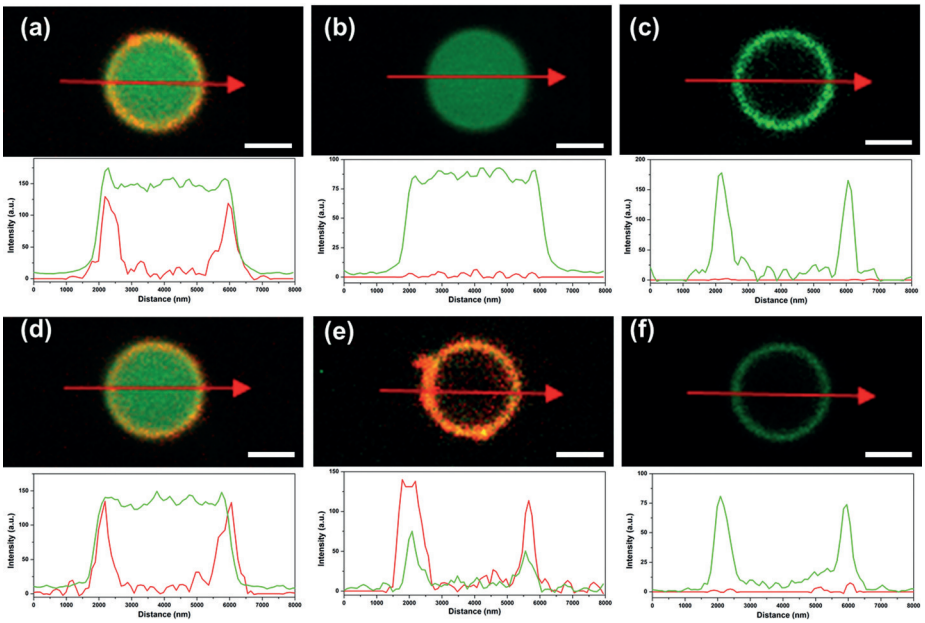

Figure 4. a)–c) Sequential release from the shell, and then from the core: a) before release, b) release of Nile Red by increasing temperature, c) subsequent release of FITC-Dextran by decreasing pH from 7 to 5. d)–f) Sequential release from the core, and then from the shell: d) before release, e) pH-induced release of FITC-Dextran, f) subsequent release of Nile Red induced by temperature. The plot below each panel is the representative fluorescent intensity profile over the microcapsule.

undergoing uniform transitions during this two-stage, temperature-pH transformation (Supporting Information, Figure S8). In this way, the sequential release of hydrophobic and then hydrophilic molecules was successfully achieved.

Moreover, the release sequence of hydrophobic and hydrophilic molecules from the shell and core regions can be completely reversed by changing stimulus sequence. When pH is used as the first stimulus (decrease from 7 to 5), complete release of hydrophilic FITC-dextran component from the microcapsule interior is achieved (Figure 4 d,e). Significantly, Nile Red remains encapsulated in the shell without significant losses during this release step. Temperature is then used as the second independent stimulus to induce the release of hydrophobic Nile Red from the shell (Figure 4 f). Again, the microcapsules remain robust and stable after the sequential encapsulation and double release steps. Overall, the ratio of release components from the interior and shell depends upon dimensions of different compartments: shells thickness and interior diameter. In current design, cargo molecules release from interior is dominant, but overall this ratio is highly tunable, because both the permeability change with pH and overall shell thickness, which are directly related to the amount of encapsulated components, can be tuned in a large range (interior diameter from 100 nm to 10 μm vs. shells thickness from 10 nm to 500 nm).

The release kinetics of dye molecules from the shell and interior of microcapsules was also measured (Supporting Information). As can be seen from Figure S9, the releases from shell and interior have quite different kinetics, and the release of FITC-dextran from interior is much slower than that of Nile Red from the shell. Both releases follow first order kinetics behavior, and the quantitative analysis shows that FITC-dextran release rate constant is 0.90 h^{-1}, and a half-life time of 0.77 h. On the other hand, Nile Red release from shells has a much higher rate constant of 17.30 h^{-1}, and shorter half-life time of 0.04 h. We suggest that the release from microcapsule interior mainly depends on the physical osmotic pressure and diffusion through dense shells; therefore, the kinetics of this release process is much slower.

Such pre-programmed, reversible, and independent release of components with very different solubility (hydrophobic and hydrophilic) under different orthogonal stimuli (chemical, pH and physical, temperature) and in two opposite paths is a unique feature of our microcapsule systems. The multi-block and stimuli-responsive nature of the building blocks exploited for shell construction allows the independent transformations: temperature-triggered intramolecular morphology changes is responsible for release of hydrophobic components from SGQP, while pH-triggered intermolecular interaction changes is responsible for shell morphology and permeability changes that induces the release of hydrophilic cargo molecules from the microcapsule interior.

The stimuli-responsive, multi-step encapsulation and release is a non-trivial and very challenging task, and has not been fully demonstrated until now, despite efforts that involved micelles,[45] liposomes,[46] and polymersomes.[22,47] It is important to note that the star block copolymers are covalently bonded 3D nanocarriers with superior stability during loading and release processes as compared to the non-covalent weakly bonded systems that are typically explored. The star multiblock systems suggested here can be used to encapsulate different types of molecules within different layers, allowing for multiple drugs to be conveniently encapsulated.[48] The robust multicompartmental microcapsules demonstrated here show promising potential applications in multi-drug, multi-gene, and pre-programmed delivery, self-healing materials, and responsive multi-microreactors.

Acknowledgements

This study is supported by the National Science Foundation DMR 1505234 and CBET-1402712 grants, and the Air Force Office for Scientific Research, FA9550-14-1-0269 Award.

Keywords: dual orthogonal response · microcapsules · programmable release · star polymers · stimuli-responsive materials

How to cite: *Angew. Chem. Int. Ed.* **2016**, *55*, 4908–4913
Angew. Chem. **2016**, *128*, 4992–4997

[1] J. Cui, M. P. van Koeverden, M. Müllner, K. Kempe, F. Caruso, *Adv. Colloid Interface Sci.* **2014**, *207*, 14–31.
[2] W. Xu, I. Choi, F. A. Plamper, C. V. Synatschke, A. H. Müller, V. V. Tsukruk, *ACS Nano* **2013**, *7*, 598–613.
[3] W. Tong, X. Song, C. Gao, *Chem. Soc. Rev.* **2012**, *41*, 6103–6124.
[4] N. J. Shah, B. B. Hsu, E. C. Dreaden, P. T. Hammond in *Layer-by-Layer Films for Biomedical Applications*, *Vol. 7* (Eds.: C. Picart, F. Caruso, J. C. Voegel), Wiley-VCH, Weinheim, **2014**, pp. 133–170.
[5] M. N. Antipina, G. B. Sukhorukov, *Adv. Drug Delivery Rev.* **2011**, *63*, 716–729.
[6] W. Xu, P. A. Ledin, V. V. Shevchenko, V. V. Tsukruk, *ACS Appl. Mater. Interfaces* **2015**, *7*, 12570–12596.
[7] M. Delcea, H. Möhwald, A. G. Skirtach, *Adv. Drug Delivery Rev.* **2011**, *63*, 730–747.
[8] B. M. Wohl, J. F. Engbersen, *J. Controlled Release* **2012**, *158*, 2–14.
[9] H. Bysell, R. Månsson, P. Hansson, M. Malmsten, *Adv. Drug Delivery Rev.* **2011**, *63*, 1172–1185.
[10] M. Delcea, A. Yashchenok, K. Videnova, O. Kreft, H. Möhwald, A. G. Skirtach, *Macromol. Biosci.* **2010**, *10*, 465–474.
[11] M. Marguet, C. Bonduelle, S. Lecommandoux, *Chem. Soc. Rev.* **2013**, *42*, 512–529.
[12] O. Kreft, A. G. Skirtach, G. B. Sukhorukov, H. Möhwald, *Adv. Mater.* **2007**, *19*, 3142–3145.
[13] H. Bäumler, R. Georgieva, *Biomacromolecules* **2010**, *11*, 1480–1487.
[14] J. Shi, L. Zhang, Z. Jiang, *ACS Appl. Mater. Interfaces* **2011**, *3*, 881–889.
[15] B. V. Parakhonskiy, A. M. Yashchenok, M. Konrad, A. G. Skirtach, *Adv. Colloid Interface Sci.* **2014**, *207*, 253–264.
[16] J. Zhang, R. J. Coulston, S. T. Jones, J. Geng, O. A. Scherman, C. Abell, *Science* **2012**, *335*, 690–694.
[17] A. Abbaspourrad, N. J. Carroll, S. H. Kim, D. A. Weitz, *J. Am. Chem. Soc.* **2013**, *135*, 7744–7750.
[18] M. Windbergs, Y. Zhao, J. Heyman, D. A. Weitz, *J. Am. Chem. Soc.* **2013**, *135*, 7933–7937.
[19] L. Liu, J. P. Yang, X. J. Ju, R. Xie, Y. M. Liu, W. Wang, J. J. Zhang, C. H. Niu, L. Y. Chu, *Soft Matter* **2011**, *7*, 4821–4827.
[20] H. Zhang, E. Tumarkin, R. Peerani, Z. Nie, R. M. A. Sullan, G. C. Walker, E. Kumacheva, *J. Am. Chem. Soc.* **2006**, *128*, 12205–12210.
[21] C. X. Zhao, *Adv. Drug Delivery Rev.* **2013**, *65*, 1420–1446.
[22] R. Chandrawati, M. P. van Koeverden, H. Lomas, F. Caruso, *J. Phys. Chem. Lett.* **2011**, *2*, 2639–2649.
[23] B. S. Kim, S. W. Park, P. T. Hammond, *ACS Nano* **2008**, *2*, 386–392.
[24] W. Xu, P. A. Ledin, F. A. Plamper, C. V. Synatschke, A. H. Müller, V. V. Tsukruk, *Macromolecules* **2014**, *47*, 7858–7868.
[25] I. Choi, S. T. Malak, W. Xu, W. T. Heller, C. Tsitsilianis, V. V. Tsukruk, *Macromolecules* **2013**, *46*, 1425–1436.
[26] Z. Iatridi, C. Tsitsilianis, *Polymer* **2011**, *3*, 1911–1933.
[27] J. J. Richardson, M. Björnmalm, F. Caruso, *Science* **2015**, *348*, aaa2491.
[28] I. Choi, D. D. Kulkarni, W. Xu, C. Tsitsilianis, V. V. Tsukruk, *Langmuir* **2013**, *29*, 9761–9769.
[29] W. Xu, P. A. Ledin, Z. Iatridi, C. Tsitsilianis, V. V. Tsukruk, *Macromolecules* **2015**, *48*, 3344–3353.
[30] K. Chen, J. Xu, J. C. Luft, S. Tian, J. S. Raval, J. M. DeSimone, *J. Am. Chem. Soc.* **2014**, *136*, 9947–9952.
[31] Z. Iatridi, Y. Roiter, N. Stavrouli, S. Minko, C. Tsitsilianis, *Polym. Chem.* **2011**, *2*, 2037–2044.
[32] Z. Iatridi, M. S. Lencina, C. Tsitsilianis, *Polym. Chem.* **2015**, *6*, 3942–3955.
[33] T. Shutava, M. Prouty, D. Kommireddy, Y. Lvov, *Macromolecules* **2005**, *38*, 2850–2858.
[34] H. Ejima, J. J. Richardson, K. Liang, J. P. Best, M. P. van Koeverden, G. K. Such, J. Cui, F. Caruso, *Science* **2013**, *341*, 154–157.
[35] J. Chen, V. Kozlovskaya, A. Goins, J. Campos-Gomez, M. Saeed, E. Kharlampieva, *Biomacromolecules* **2013**, *14*, 3830–3841.
[36] I. Erel-Unal, S. A. Sukhishvili, *Macromolecules* **2008**, *41*, 3962–3970.
[37] V. Kozlovskaya, E. Kharlampieva, I. Drachuk, D. Cheng, V. V. Tsukruk, *Soft Matter* **2010**, *6*, 3596–3608.
[38] I. Choi, R. Suntivich, F. A. Plamper, C. V. Synatschke, A. H. Müller, V. V. Tsukruk, *J. Am. Chem. Soc.* **2011**, *133*, 9592–9606.
[39] E. Kharlampieva, V. Kozlovskaya, S. A. Sukhishvili, *Adv. Mater.* **2009**, *21*, 3053–3065.
[40] A. Zhuk, S. A. Sukhishvili, *Soft Matter* **2013**, *9*, 5149–5154.
[41] J. K. Armstrong, R. B. Wenby, H. J. Meiselman, T. C. Fisher, *Biophys. J.* **2004**, *87*, 4259–4270.
[42] M. T. Popescu, C. Tsitsilianis, *ACS Macro Lett.* **2013**, *2*, 222–225.
[43] I. N. Kurniasih, H. Liang, S. Kumar, A. Mohr, S. K. Sharma, J. P. Rabe, R. Haag, *J. Mater. Chem. B* **2013**, *1*, 3569–3577.
[44] W. Xu, I. Choi, F. A. Plamper, C. V. Synatschke, A. H. Müller, Y. B. Melnichenko, V. V. Tsukruk, *Macromolecules* **2014**, *47*, 2112–2121.
[45] Z. Zhu, N. Gao, H. Wang, S. A. Sukhishvili, *J. Controlled Release* **2013**, *171*, 73–80.
[46] C. Boyer, J. A. Zasadzinski, *ACS Nano* **2007**, *1*, 176–182.
[47] H. Lomas, A. P. Johnston, G. K. Such, Z. Zhu, K. Liang, M. P. Van Koeverden, S. Alongkornchotikul, F. Caruso, *Small* **2011**, *7*, 2109–2119.
[48] A. Shukla, R. C. Fuller, P. T. Hammond, *J. Controlled Release* **2011**, *155*, 159–166.

Received: January 13, 2016
Revised: February 8, 2016
Published online: March 15, 2016

